T.3 : Magnetostructural transition and multi-functional properties in ferromagnetic shape memory alloys

Vishnu Kumar Sharma, Magnetic and Superconducting Materials Section, Materials and Advanced Accelerator Sciences Division
vishnusharma@rrcat.gov.in

1. Introduction

The ferromagnetic shape memory alloys are a focus of research activities for almost a decade due to their potential for magnetic field controlled actuation applications. Some of these alloys show a magnetic-field induced strain as large as 10% [1]. This strain is almost two orders of magnitude larger than ~0.1 % strain observed in the piezoelectric materials, and ~0.2% strain exhibited by the leading magnetostrictive material Terfenol-D. The ferromagnetic shape memory effect is closely related with the conventional temperature induced shape memory effect. A first-order displacive structural phase transition from the high temperature austenite (AST) phase to the low temperature martensite (MST) phase, also known as martensitic transition (MT), plays the key role in the shape memory effect [2]. The MST phase has a twinned microstructure. The crystallographic twins can reorient under the application of an external stress resulting in a large recoverable strain in the material. This leads to the conventional shape memory and superelasticity in materials like NiTi alloys. In a ferromagnetic MST phase with large magnetocrystalline anisotropy, an applied magnetic field can also lead to the reorientation of crystallographic twins. Such magnetic field controlled reorientation of MST twins [3] is responsible for the large magnetic field induced strain of the order of 10% observed in some Ni-Mn-Ga based alloys [1]. Though the Ni-Mn-Ga based ferromagnetic shape memory alloys were expected to be very promising for magnetic field controlled actuation related applications, their highly brittle nature has restricted their use in practical applications. In the search of other suitable ferromagnetic shape memory alloys, some new alloy systems have been explored. In this context, off-stoichiometric Heusler alloys Ni-Mn-X (X = In, Sn, Sb) have been identified as potential candidates for ferromagnetic shape memory effect during the last decade [4]. The austenite and martensite phases of these alloys are reported to have cubic $L2_1$ and orthorhombic crystal structures respectively. Unlike the Ni-Mn-Ga alloys, where the difference between magnetization of the MST and AST phases is not large, the MT in these Ni-Mn-X alloys is accompanied with a large decrease in magnetization. This magneto-structural transition can be induced by temperature (T) as well as magnetic field (H).

Despite the fact that a first order phase transition (FOPT) plays a crucial role in conventional/ferromagnetic shape memory effect, studies on the underlying FOPT are very scarce. The Magnetic and Superconducting Materials Section (M&SMS) of RRCAT has been studying FOPTs in various materials for quite some time. It was anticipated in the M&SMS that the magnetic-field induced MST-AST phase transition in Ni-Mn-X alloys is likely to give rise to appreciable changes in various thermodynamic and transport properties. This in turn was expected to lead to newer and interesting functionalities of technological importance in these alloys apart from the shape memory effect. The aim of the present study has been to understand the underlying physics of the FOPT in Ni-Mn-In based ferromagnetic shape memory alloys, and to explore the potential of these alloys for technological applications. Detailed experimental investigation has been carried out in Ni-Mn-In off-stoichiometric Heusler alloys at the M&SMS. It has been found that the phase transition in these alloys is a disorder-influenced FOPT. These alloys had been found to exhibit technologically important functional properties like the giant magneto-caloric effect (MCE), giant magneto-resistance and the giant magneto-striction whose temperature regime can be tuned suitably. Magnetic refrigeration using the MCE in solids has attracted attention because of its higher efficiency and environment friendly nature in comparison to the conventional vapour compression cycle [5]. Materials showing giant MCE are also proposed as regenerators in cryogenic applications. Magneto-strictive materials can be used for linear and rotational motion control with practical applications in tuning of superconducting radio frequency cavities [6]. These functional properties of the material under investigation are therefore of substantive relevance to the ongoing research and development activities carried out at RRCAT.

2. Phenomenology of first order phase transitions

Phase of a material is defined as a region of spatially uniform macroscopic properties like density, crystal structure, magnetic order etc. The transition from one phase to the other, due to change in a control variable (temperature, pressure, magnetic field etc.), is termed as a phase transition.

In the Ehrenfest's scheme, a transition is said to be of n^{th} order if the n^{th} order derivative of the Gibbs free energy (G) with respect to extensive thermodynamic variables is discontinuous. Thus, a first order phase transition is identified as that which involves discontinuity in the first order derivative of free energy [7]. This is shown schematically in Fig.T.3.1 where entropy S (which is first order derivative of free energy with respect to temperature) and volume V (which is first order derivative of free energy with respect to pressure P) are discontinuous across the transition. An entropy discontinuity results in latent heat of the transition. Similarly, discontinuity in magnetization (which is the first order derivative of free energy with respect to magnetic field) identifies a first order magnetic phase transition.

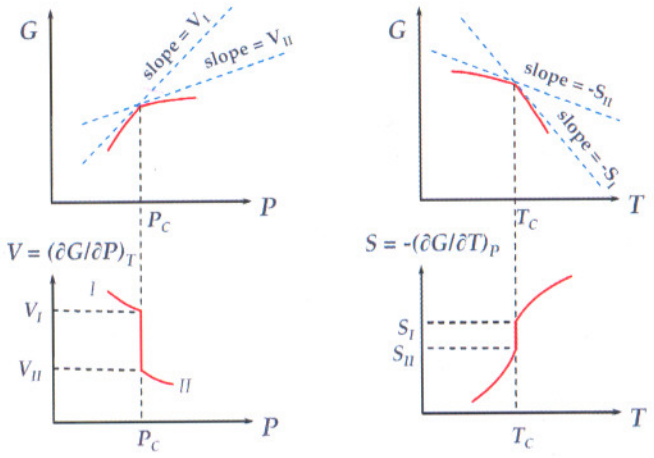

Fig. T.3.1. Variation of free energy with temperature and pressure across a first order phase transition. First order derivatives of free energy, volume and entropy, are discontinuous across the transition.

Most of the transitions which do not have a latent heat (hence are not FOPT) show either a divergence or a cusp, instead of a discontinuity, in heat capacity (2nd derivative of G with respect to temperature), and hence do not fit in the Ehrenfest's scheme. A more general classification of phase transitions is based on variation of order parameter across the transition. Order parameter is a chosen entity which is zero in high temperature phase and is non-zero in low temperature phase, indicating some sort of ordering across the transition. The transitions across which the order parameter grows discontinuously from zero, are termed as discontinuous phase transition (these are the FOPT in the Ehrenfest's scheme). Other transitions involving continuous growth of order parameter across the transition are called as continuous phase transitions (these include the second and higher order phase transitions of the Ehrenfest's scheme).

A detailed description of phase transition in terms of order parameter is provided by the Landau theory [8, 9]. The Landau theory expresses the free energy as an analytical function in terms of a power series of order parameter assuming that the order parameter is small and uniform near the phase transition. The form of free energy as a function of order parameter suitable for first order magnetic transitions which involves only even powers of order parameter is shown at different temperatures in Fig. T.3.2. The equilibrium phase is determined from the minimum in free energy.

The free energy function in Fig. T.3.2 has two minima at T_c with $\Psi=0$ and $\Psi\neq0$ with equal free energy values, where Ψ is the order parameter. This temperature is known as the thermodynamical transition temperature. At T_c, the order parameter grows discontinuously which qualifies the transition as an FOPT. Thermodynamically, the phase transition should occur at T_C. However, during cooling, the high temperature $\Psi=0$ (disordered state) phase is stable against small energy fluctuations as there is a barrier between the $\Psi=0$ and the $\Psi\neq0$ (ordered) state A sufficiently large energy fluctuation can convert this high temperature phase to low temperature $\Psi>0$ phase. So, high temperature phase is a metastable phase. At a temperature T^* the high temperature state can no longer remain as metastable as the barrier is between the ordered and disordered state is zero and an infinitesimal fluctuation will complete the transformation. The temperature T^* is thus known as the limit of metastability of the high temperature phase while cooling, and the higher temperature phase can be supercooled down to T^*. Similarly the low temperature phase can remain as a metastable phase up to T^{**} while heating and the system can be superheated up to T^{**}. Thus Landau theory predicts a thermal hysteresis across a FOPT. This also predicts an entropy discontinuity and latent heat [9].

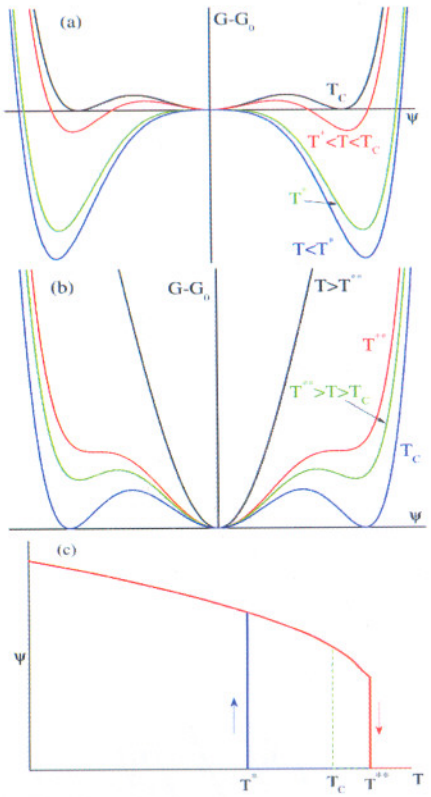

Fig. T.3.2. Variation of Landau free energy with order parameter at different temperatures across a first order transition: (a) while decreasing temperature and (b) while increasing temperature, with (c) a thermal hysteresis in order parameter. G_0 is the free energy not related with order parameter.

Influence of disorder on the first order phase transition:

In a perfectly pure system, an FOPT has a single T_C as shown by the thick dashed line in the schematic of Fig. T.3.3(a). As discussed above, such a system can be supercooled through careful cooling. In that case the phase transition during cooling follows the solid line marked by T_3-T^* [10]. Similarly, the system can be superheated and follows the solid line T_1-T^{**} during heating. The entire sample transforms at a single temperature, $T_3 = T^*$ while cooling and $T_1 = T^{**}$ while heating. Small amount of disorder in the sample can diffuse the transition, and the system follows the dotted curves T_{3a}-T_4-T^* and T_{1a}-T_2-T^{**} during cooling and warming respectively. In such a case the two phases can coexist over certain temperature range. Microscopic random-quenched disorder in a sample leads to a landscape of transition temperature across the volume of the sample [11]. In the presence of a large amount of such disorder, the sharpness of the FOPT smears out to a large extent. The thick dashed line of Fig. T.3.3(b) represents such a transition. In the presence of supercooling and superheating, the phase transition will follow the solid curves T_3-T_4-T^* and T_1-T_2-T^{**} while cooling and heating respectively. In such a disorder-influenced FOPT, the onset of the low-temperature phase during cooling can take place at a temperature which is higher than the onset of the high-temperature phase during warming [10]. It is worth noticing here that in such cases the latent heat across the FOPT might be difficult to observe experimentally, and thermal hysteresis can be used as a qualifying criterion for an FOPT [7].

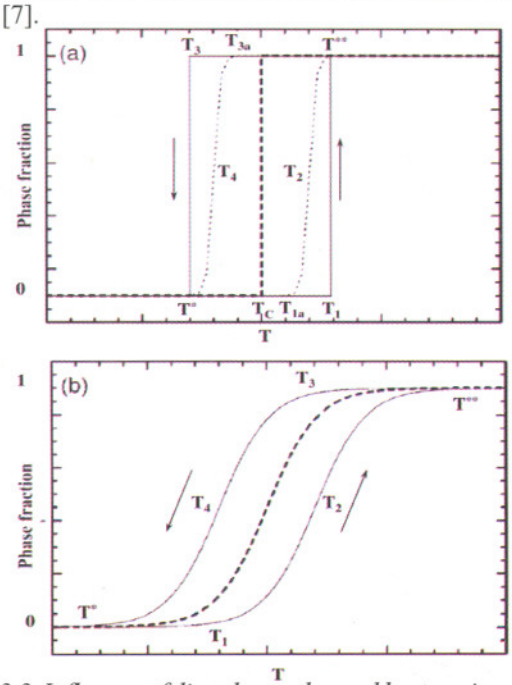

Fig.T.3.3. Influence of disorder on thermal hysteresis across a first order phase transition: variation of phase fraction of high temperature phase in (a) a pure system and that with small amount of disorder, and (b) system with large amount of disorder.

3. The martensite-austenite phase transition in Ni-Mn-In based alloys

With this phenomenological background on FOPT, we now discuss the studies in Ni-Mn-In based alloy systems. The results of isofield T dependence and isothermal H dependence of magnetization (M) measurements on a representative sample $Ni_{50}Mn_{34}In_{16}$ are presented in Fig. T.3.4(a). While cooling from 350 K in H= 10 kOe, magnetization increases with decreasing temperature. This is related with paramagnetic (PM) to ferromagnetic (FM) transition in the alloy with the Curie temperature of ~305 K [12]. With further lowering of temperature, there is a rapid fall in M around 240 K. Magnetization again increases with further lowering of T below 200 K. Also, there is a thermal hysteresis in M. The sharp decrease in M around 240 K and thermal hysteresis are related to the martensitic transition occurring in this alloy [13]. This change in magnetization is probably related to the change in exchange interaction across the transition because of different lattice parameters in AST and MST phases. In off-stoichiometric Heusler alloys Ni-Mn-X, there exists an incipient antiferromagnetic (AFM) coupling between the magnetic moments of the excess Mn atoms and the magnetic moments of the Mn atoms occupying sites corresponding to the stoichiometric composition. This incipient AFM coupling can be strengthened further in the MST phase resulting in lower magnetization. However, both MST and AST phases possess overall ferromagnetic character [14].

The four characteristic temperatures, martensite-start (T_{MS}), martensite-finish (T_{MF}) while cooling, and austenite-start (T_{AS}) and austenite-finish (T_{AF}) while warming in H=10 kOe, are marked in Fig. 4(a). It has been found that all these four characteristic temperatures shift towards the lower T side with increasing H [15] (e.g. compare 10 kOe and 50 kOe M-T curves in Fig. T.3.4) indicating a possibility of field induced transition.

Isothermal $M(H)$ curves (presented in Fig. T.3.4(b)) of the alloy are reversible in the T-regime away from the MT region. In the phase coexistence regime of AST to MST phase transition, the isothermal $M(H)$ curves exhibit a marked hysteresis. This hysteresis is not related to the ferromagnetic character of MST and AST phases but is a result of the H-induced FOPT from MST phase to AST phase [15]. In a ferromagnetic material, the hysteresis arises due to domain wall pinning and/or anisotropy and has a maximum width at $H = 0$. In such a case, the width of the hysteretic region increases with the lowering of temperature. But in the present case, the width of hysteresis is almost zero at $H = 0$, and the hysteresis

vanishes both on the lower and higher temperature sides of the MT regime. Similar magnetic field induced MST-AST transitions have also been observed in $Ni_{50}Mn_{34.5}In_{15.5}$ [16], $Ni_{50}(Mn,1\%Cr)_{34}In_{16}$ [17], $Ni_{50}(Mn,2\%Cr)_{34}In_{16}$ [17] and $(Ni,2\%Cu)_{50}Mn_{34}In_{16}$ [18] alloys as well. It should be noted from the comparison of Figs. T.3.3(b) and T.3.4(a) that T_3 $(=T_{MS}) > T_1$ $(=T_{AS})$, which suggests the disorder-influenced first order nature of MST-AST the transition in $Ni_{50}Mn_{34}In_{16}$. (see discussion related to Fig. T.3.3(b)). A similar relation between onset fields is also true for the H- induced transition shown in Fig. T.3.4(b).

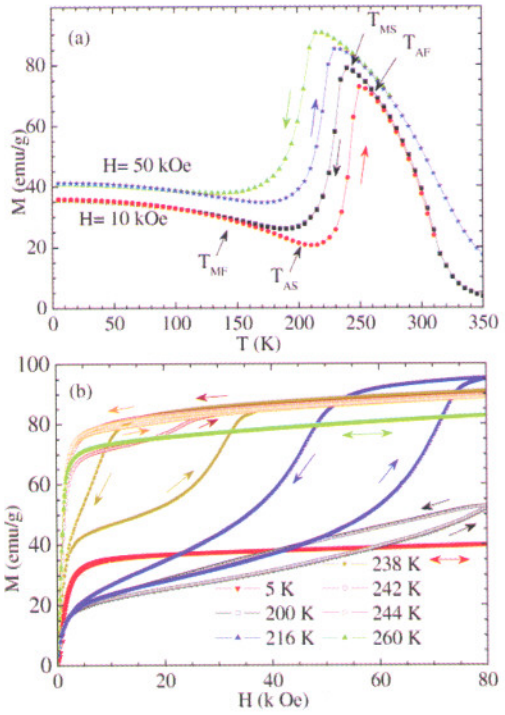

Fig. T.3.4. (a)Temperature dependence of magnetization of $Ni_{50}Mn_{34}In_{16}$ alloy in field of 10 and 50 kOe. (b) Isothermal magnetic field dependence of magnetization of the same alloy at various temperatures. Arrows indicate direction of temperature/field change.

Disorder-influenced nature of the martensite-austenite phase transition in $Ni_{50}Mn_{34}In_{16}$:

Phase coexistence and hysteresis are generic features of a disorder-influenced first-order phase transition [19]. The visual evidence of phase coexistence across the MST-AST phase transition in $Ni_{50}Mn_{34}In_{16}$ alloy has been obtained through scanning Hall probe (SHP) imaging of the magnetic field induced MST–AST phase transition in this alloy [20]. SHP imaging was performed at 236 K. Two different protocols were adopted to reach the temperature 236 K, as shown in the H-T phase diagram in Fig. T.3.5 (variation of T_{MS}, T_{MF}, T_{AS} and T_{AF} with magnetic field constitute the H-T phase diagram). In the protocol P1, the sample was cooled from 300 K in zero magnetic field down to 236 K without undershooting the target temperature. Then SHP imaging was performed in different fields at constant temperature. In the protocol P2, the sample was cooled in zero magnetic field from 300 K to 30 K. Then the sample was warmed up to 236 K without overshooting the target temperature, and subsequently the SHP imaging was performed at constant temperature. The Hall voltage is converted to colour scale and the resultant images are presented in Fig. T.3.5.

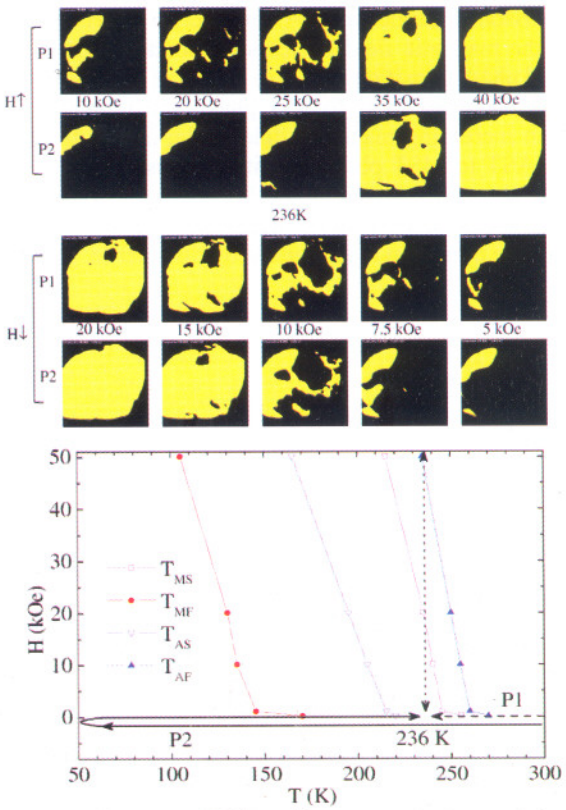

Fig. T.3.5. Scanning Hall probe images in increasing (H↑) and decreasing(H↓) magnetic field across the field induced transition in $Ni_{50}Mn_{34}In_{16}$ alloy. H-T phase diagram of the alloy in the lower panel depicts the paths followed in the protocols P1 and P2 to reach 236 K.

In Fig. T.3.5, the yellow regions represent the AST phase, and the black regions show the MST phase. At start of the experimental cycle in both protocols in H=10 kOe, some portions of the images show yellow colour indicating that the MST to AST phase transition has started in these regions of the sample. The amount of the AST phase in $H = 10$ kOe is

clearly larger in protocol P1. With increasing H, newer yellow patches appear and the existing yellow patches grow in area indicating the nucleation and growth of the AST phase. The entire sample is yellow in 40 kOe magnetic field for both the protocols P1 and P2. In the decreasing field cycle, the MST phase appears as black spots and the nucleation and growth of the MST phase is clearly seen. The nucleation and growth kinetics of the AST to MST phase transition in both the protocols P1 and P2 appear to be quite similar as the field is decreased from 40 kOe to zero. Some AST phase remains untransformed in fields down to 5 kOe in both the protocols. Fig. T.3.5 actually shows the snap-shots of the coexistence of MST and AST phases on the length scale of tens of micrometers, extended over a very wide regime of magnetic field. Comparison of the increasing-H and decreasing-H cycles also show the magnetic field hysteresis associated with this *H*-induced phase transition. It is also observed that the region of sample where the MST to AST phase transition starts first (last) in increasing magnetic field cycle, is also the region where AST to MST phase transition starts at last (first) in decreasing magnetic field cycle. This shows that the hysteresis associated with the magnetic field induced MST-AST phase transition is influenced by disorder (e. g. defects, dislocations).

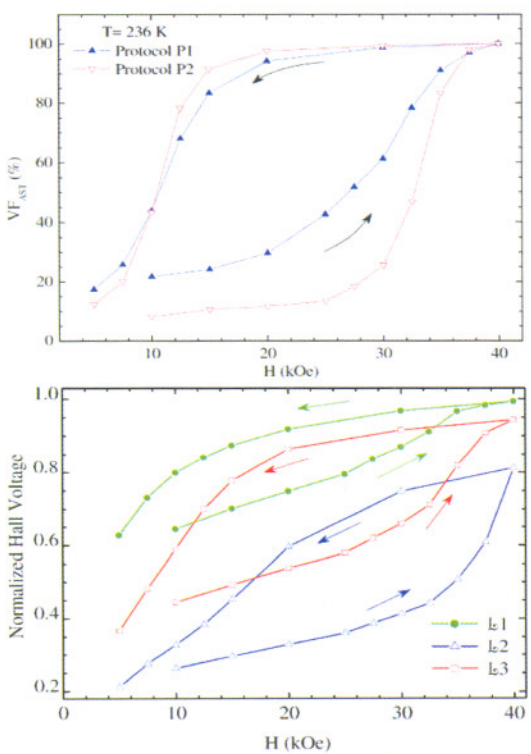

Fig. T.3.6. Variation of austenite volume fraction, estimated from Hall images, with magnetic field in the protocols P1 and P2. Lower panel shows variation of local Hall voltage at representative locations across the sample.

Magnetic field dependence of the volume fraction of the AST phase, estimated from the scanning Hall probe images [20], is presented in Fig. T.3.6. In the increasing magnetic field cycle, the amount of AST phase is larger in protocol P1. Fig. T.3.6 clearly depicts the difference in the onset fields of the MST to AST phase transition in the protocols P1 and P2 with increasing magnetic field. Thus the nature of the magnetic field induced MST to AST phase transition in the $Ni_{50}Mn_{34}In_{16}$ alloy seems to be affected by the thermomagnetic history (TMH) of the sample.

Local magnetic behaviour of the sample across the magnetic field driven MST-AST phase transition had been studied by tracking the Hall voltage signal coming from the individual pixels which corresponds to 10 μm × 10 μm sample area approximately. The magnetic field dependence of such a voltage signal produces a local Hall voltage loop. Lower panel in Fig. T.3.6 presents the local Hall voltage loops corresponding to three representative sites (pixels, named as L1, L2, and L3) on the sample. The Hall voltages in the local loops are normalized to the Hall voltage at the site L1 in 40 kOe magnetic field. It is interesting to observe that while the magnetic field induced MST to AST phase transition is completed well below 40 kOe at the site L1, the transition is probably not completed at the site L2 at $H = 40$ kOe. On the other hand, the transition is very near to completion at the site L3 in the same field value. The characteristics exhibited by the local Hall voltage loops indicate the presence of a landscape of critical magnetic field for MST-AST phase transition across the sample. This confirms the disorder-influenced nature of this magnetic field induced MST-AST phase transition in $Ni_{50}Mn_{34}In_{16}$ as inferred from shape of isofield M(T) and isothermal M(H) curves.

4. Multifunctional properties in NiMnIn based alloys

The H-induced transition in Ni-Mn-In based alloys exhibit various functional properties that include magnetoresistance (MR), magnetocaloric effect (MCE) and field induced strain (FIS).

MR was calculated as the relative change in resistivity under application of magnetic field. It was found that both the AST and MST phases show negative MR because of the decrease in spin disorder scattering in ferromagnetic state with applied magnetic field. A relatively large MR is observed in the MT region (see Fig. T.3.7) in the $Ni_{50}Mn_{34}In_{16}$ alloy. This MR arises from the magnetic field induced MST to AST phase transition. An MR of about 45 % is observed at 250 K in field of 10 kOe, that increases with magnetic field, and in 50 kOe magnetic field 64% MR is observed at 230 K [21]. Similar MR has been observed in our $Ni_{50}Mn_{34.5}In_{15.5}$ alloy also [16].

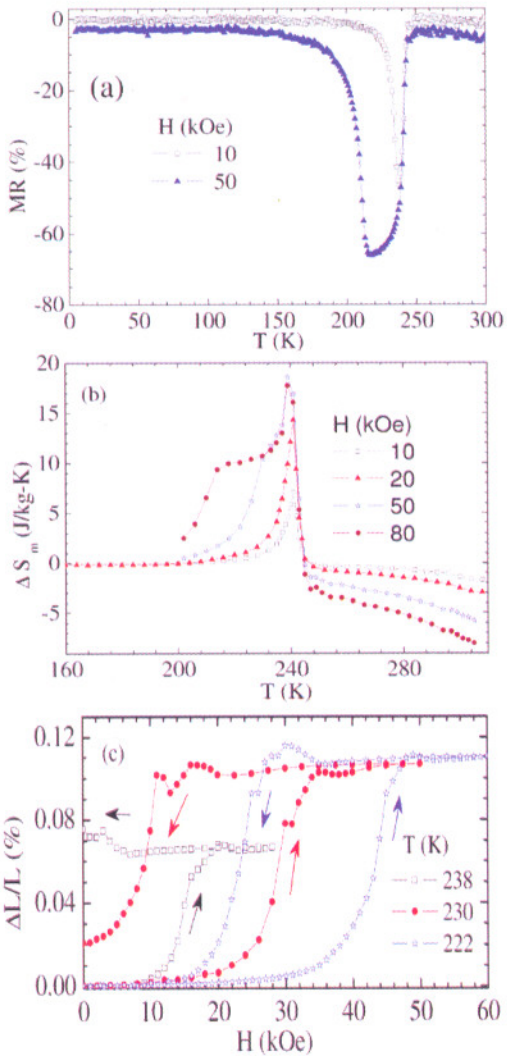

Fig. T.3.7. Multifunctional properties in $Ni_{50}Mn_{34}In_{16}$ alloy: temperature dependence of (a) magneto-resistance, (b) isothermal entropy change, and (c) magnetic field induced strain.

The MCE has been estimated as isothermal change of magnetic entropy (ΔS_M) using Maxwell's thermodynamic relations [22]. Temperature dependence of ΔS_M for different magnetic field excursions is shown in Fig. T.3.7(b) for $Ni_{50}Mn_{34}In_{16}$. The $\Delta S_M(T)$ peaks around the AST–MST phase transition regime, and its sign is positive, which means that the sample temperature decreases by the adiabatic increase of magnetic field. At a temperature above the AST–MST phase transition regime, $\Delta S_M(T)$ changes sign and becomes negative as expected in the conventional MCE. The maximum of $\Delta S_M \approx$ 19 J/kg-K occurs in H= 50 kOe around 240 K [23].

The FIS in $Ni_{50}Mn_{34}In_{16}$ alloy has been measured using the strain gauge technique as relative length change ($\Delta L/L$) with respect to length in zero field. Fig. T.3.7 (c) presents the FIS at various temperatures. The large rise and associated magnetic field hysteresis in the $\Delta L/L(H)$ curve are related with magnetic field induced transition from the MST phase to the AST phase. Appreciable FIS of nearly 0.1% has been obtained in the $Ni_{50}Mn_{34}In_{16}$ alloy in certain T regime across the transition [24]. Reversible FIS is equivalent to ferromagnetic shape memory effect whose mechanism is different from the MST variant reorientation.

Thermomagnetic history effects in functional properties:

The interesting functional properties observed in $Ni_{50}Mn_{34}In_{16}$ alloy arise from the first-order MST-AST phase transition. SHP imaging experiment established that this MST-AST phase transition is a disorder influenced first-order phase transition, and the volume fractions of AST and MST phases depend on the TMH of the sample. As a result, the functionalities are also expected to be dependent on the TMH of the sample. Such TMH-dependence of functional properties have been explored by measuring the functional properties in different protocols [25, 26]. Protocols P1 and P2 (explained in SHP imaging experiment) were adopted to

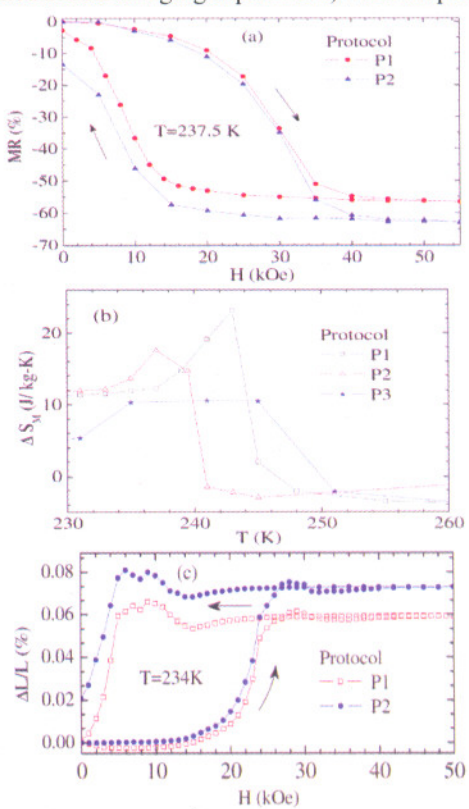

Fig. T.3.8. Theromagnetic history dependence of functional properties in $Ni_{50}Mn_{34}In_{16}$ alloy: (a) Magnetoresistance, (b) magnetocaloric effect, and (c) magnetic field induced strain.

explore TMH dependence in MR and FIS. For MCE, apart from P1 and P2, a third protocol was also adopted. In this third protocol P3, once measurements are over at a temperature, the sample was just warmed to next temperature for measurement.

MR measured at 237.5 K is presented in Fig. T.3.8(a). In both the protocols P1 and P2, the MR is negative. However, the magnitude as well as the reversibility of MR depends on the thermomagnetic history of the sample. The magnitude of ΔS_M as a function of temperature estimated for a magnetic field excursion from zero to 80 kOe is shown in Fig. T.3.8(b). It is clearly seen that the maximum obtainable value of MCE depends on the protocol of the measurement. The *ΔL/L(H)* measurements performed at 234 K are presented in Fig T.3.8(c)). The magnetic field induced strain is larger in protocol P2. The zero-field strain value is completely recoverable in protocol P1 while it is only partially recoverable in protocol P2. All these observations highlight the importance of TMH for practical use of the alloy.

Tuning the useful temperature regime of multifunctional properties:

The functional properties discussed above, can have more technological importance if the T-range of the MST-AST transition can be shifted towards the room temperature.

The MT transition temperature in the Ni-Mn-X alloys can be increased by: (i) increasing the *e/a* (electrons per atom) ratio [27, 28], and (ii) applying external pressure [29]. The effect of applying pressure can be simulated by substituting the atoms by a smaller atom. Therefore the substitution of an atom in Ni-Mn-X alloy by relatively smaller isoelectronic atom is expected to shift the martensitic transition towards the higher temperature side. Further if the substituted and substituent atoms are not isoelectronic, the e/a ratio will also change.

For tuning the *T*-regime of functional properties, we have prepared new alloys by substituting Mn by Cr and Fe, and substitution of Ni by Cu in $Ni_{50}Mn_{34}In_{16}$ alloy. The partial substitutions of Mn by Cr [17] and Ni by Cu [18] are found to increase the MT temperature as compared to that in parent alloy. On the other hand, with substitution of Mn by Fe the MT temperature is found to decrease [17]. The *T*-regime of MCE which is near 240 K in $Ni_{50}Mn_{34}In_{16}$ increases to near 270 in $Ni_{50}(Mn,1\%Cr)_{34}In_{16}$ [30] and near room temperature in $Ni_{50}(Mn,2\%Cr)_{34}In_{16}$ alloy [31]. The substitution of Cu in the Ni site also raises the *T*-regime of functionalities from 240 K to near room temperature [18]. The multifunctional properties of the Cu doped alloy are presented in Fig.T.3.9. Magnetoresistance of nearly 50%, isothermal entropy change of nearly 25 J/kg-K under the application of 45 kOe field, and magnetic field induced strain of nearly 0.06% are exhibited by the alloys. Not only the functional properties are comparable with that of the parent alloy, but also the temperature regime has come near to ambient temperatures. The application of hydrostatic pressure on $Ni_{50}Mn_{34}In_{16}$ alloy also pushes the MT and multifunctional properties towards the higher temperature [32].

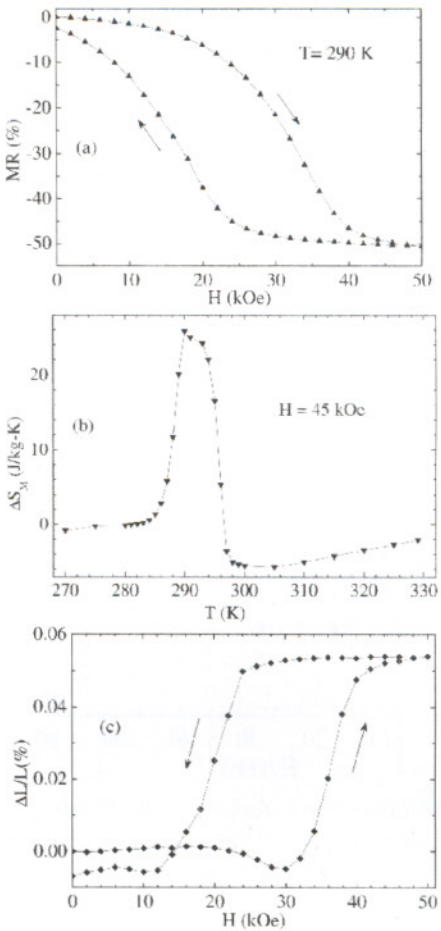

Fig. T.3.9. Near room temperature multifunctional properties in $(Ni,2\%Cu)_{50}Mn_{34}In_{16}$ alloy: (a) magnetoresistance, (b) magnetocaloric effect, and (c) magnetic field induced strain.

5. Non-equilibrium dynamics of austenite to martensite transition

Some of the Ni-Mn-In alloys were found to show non-equilibrium dynamics across the AST to MST transition. For example, Fig. T.3.10 presents M vs. T plots for $Ni_{50}Mn_{34}In_{16}$ obtained in zero field cooled (ZFC) warming, field cooled cooling (FCC), and field cooled warming (FCW) protocol in the presence of different applied fields. In the ZFC warming

protocol, the sample is first cooled from 350 K down to lowest temperature of measurement in zero magnetic field. The magnetic field is then switched ON and the measurements are done while warming the sample in presence of applied field. In FCC protocol, magnetic field is applied at 350 K, and measurement is performed while cooling the sample in presence of magnetic field. After the FCC protocol, the measurements are performed in FCW protocol while warning the sample in presence of magnetic field.

In Fig. T.3.10, the thermomagnetic irreversibility (TMI) between $M_{ZFC}(T)$ and $M_{FCC}(T)$ first decreases with the increase in H. This behaviour can be explained in terms of the hindrance of domain wall motion in the martensite FM phase which is normal to all ferromagnets. However, in higher fields, $M_{ZFC}(T)$ again bifurcates from $M_{FCC}(T)$ and the TMI increases with the increasing H. This is quite anomalous behaviour, and cannot be explained in terms of TMI occurring in a feromagnet or spin glass. Similar behaviour which was earlier observed across the first-order FM to AFM phase transition in other alloys and compounds [33] has been explained in terms of kinetic arrest of the first-order FM to AFM transition resulting in a glass-like non-ergodic magnetic state [33]. In contrast to the canonical spin-glass (where the spin-configuration is random in nature, similar to a paramagnet frozen in time), the magnetic configuration in this magnetic-glass consisted of a phase coexistence of FM and AFM clusters frozen in time [33].

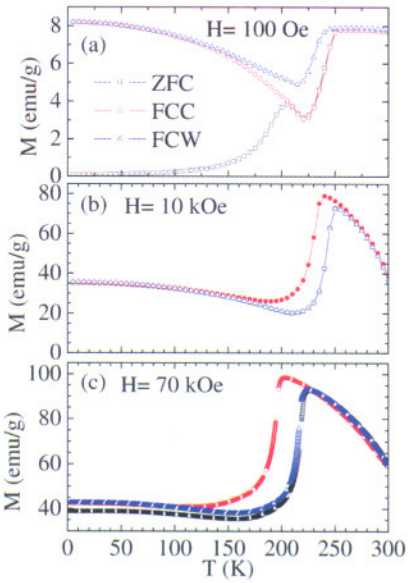

Fig. T.3.10. Variation of thermomagnetic irreversibility between ZFC and FCC magnetization curves in $Ni_{50}Mn_{34}In_{16}$ alloy with increasing magnetic field.

With similar arguments, one concludes that in high magnetic field, the first-order AST to MST phase transition in $Ni_{50}Mn_{34}In_{16}$ is not completed, but is kinetically arrested. The low T state thus obtained in the FCC mode is not an equilibrium state. It consists of converted phase fractions of equilibrium MST phase coexisting with the metastable phase fractions of the higher temperature AST phase. On the other hand, the ZFC state in which the low temperature values of $M_{ZFC}(T)$ are distinctly lower than $M_{FCC}(T)$, is the equilibrium state with MST phase only. This had been supported by temperature cycling which introduces energy fluctuation, and the FCC magnetization approaches ZFC value [34].

Results of magnetization relaxation study further support the existence of the low T glass-like magnetic state in $Ni_{50}Mn_{34}In_{16}$ alloy. Fig. T.3.11 presents M vs. time (t) plots at various temperatures on the FCC path across the AST-MST phase transition with H kept fixed at 80 kOe. A considerable relaxation in M is expected at 180 K due to the expected metastability (arising from FOPT) across the AST-MST transition. With the decrease in temperature the relaxation rate decreases continuously. However, a distinct relaxation can be observed even down to 70 K and below. The $M(t)$ data below 150 K can be fitted with Kohlrausch-Williams-Watt (KWW) stretched exponential function, which implies that the metastable state relaxes with a distribution of relaxation times [35]. The inset of Fig. T.3.11 shows a typical example of such KWW fitting. As compared to the other systems where magnetic glass has been reported, the present $Ni_{50}Mn_{34}In_{16}$ system seems to be different in the sense that both the low-H and high-H

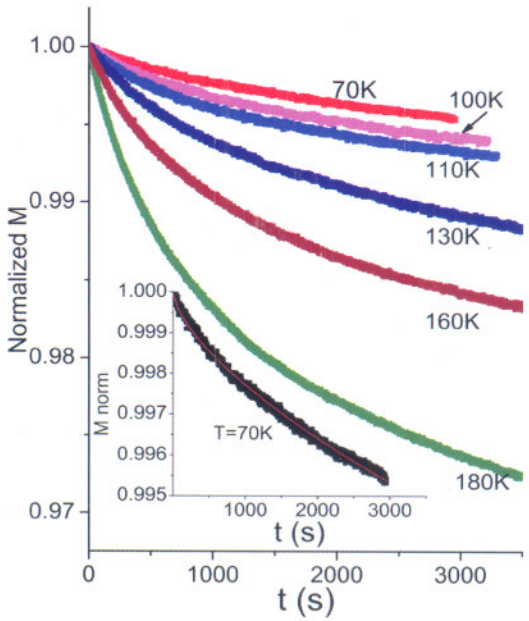

Fig. T.3.11. Relaxation of normalized magnetization at different temperatures on 80 kOe FCC curve. Inset shows fitting with KWW stretched exponential function to the relaxation at 70 K.

state involved in this *H*-induced magnetostructural transition are FM in nature [34].

Similar results had also been obtained in $Ni_{50}(Mn,1\%Fe)_{34}In_{16}$ alloy. However, it is in contrast with the parent $Ni_{50}Mn_{34}In_{16}$ alloy, where the signature of the kinetic arrest of austenite to martensite transition is observed only in fields greater than 40 kOe and the arrest is partial even in a field of 80 kOe. The kinetics of the transition in the $Ni_{50}(Mn, 1\%Fe)_{34}In_{16}$ alloy, are partially arrested even in zero (nominal) applied field and the process of transition in this alloy is completely arrested in a field of 50 kOe [17].

6. Summary

Summarizing, the martensite-austenite phase transition in Ni-Mn-In based off-stoichiometric Heusler alloys as a function of temperature and magnetic field was studied at the Magnetic and Superconducting Materials Section at RRCAT with the motivation of exploring newer functional properties of technological importance. It was established that the interesting functional properties of this alloy system, like large magnetoresistance, large magneto-caloric effect and large magnetostriction are governed by the underlying magnetic field-induced martensite-austenite transition. Scanning Hall probe imaging experiments on $Ni_{50}Mn_{34}In_{16}$ alloy has provided clear visual evidence of the coexistence of the MST and AST phases across the magnetic field-induced transition in the alloy. This supports the disorder-influenced first-order nature of the phase transition and the associated thermomagnetic history effects. These history effects are found to play an important role in the functional properties observed across this transition. The useful temperature regime of the functional properties in Ni-Mn-In based alloys can be elevated towards room temperature by chemical substitution as well as the application of hydrostatic pressure. Interesting thermomagnetic history effects were also seen where the kinetics of the austenite to martensite transition in some of the Ni-Mn-In based alloys get arrested.

These studies should provide future directions for using materials for technological applications based on first order magneto-structural martensitic phase transitions.

Acknowledgements

This work was done as a part of my thesis work. I am thankful to my thesis advisor Dr. S. B. Roy for invaluable guidance, constant support and motivation for the work. I also thank Dr. M. K. Chattopadhyay for his involvement in the work and other members of M&SMS, RRCAT for their support.

References

1. Sozinov A. et al., *Appl. Phys. Lett.* **80,** 1746 (2002)
2. Ostuka K. and Wayman C. M. *Shape Memory Materials,* (Cambridge University Press, Cambridge 1998)
3. Enkovaara J. et al. *Mater.Sci. Eng.* **A 378,** 52 (2004)
4. Sutou Y. et al., Appl. Phys. Lett. **85**, 4358 (2005).
5. Pecharsky V. K. and Gschneidner K. A. Jr., *J. Magn. Magn. Mater.* **200**, 44 (1999).
6. Mavanur A. et al., *IEEE Trans. Appl. Supercond.* **15**, 2405 (2005).
7. White R. M. and Geballe T. H., *Long range order in solids* (Academic Press, New York, 1979).
8. Reichl L. E., *A modern course in statistical physics* (John Wiley & Sons, Inc.,New York, 1998).
9. Chaikin P. M. and Lubensky T. C., *Principles of condensed matter physics* (Cambridge University Press, Cambridge, 1995).
10. Chattopadhyay M. K. et al., *Phys. Rev.* B. **68**, 174404 (2003).
11. Imry Y. and Wortis M., *Phys. Rev.* B **19**, 3580 (1979).
12. Sharma V. K. et al., *J. Phys.: Condens. Matter* **19**, 496207 (2007).
13. Krenke T. et al., *Phys. Rev.* B **73,** 174413 (2006)
14. Brown P. J., *J. Phys.: Condens. Matter* **18,** 2249 (2006)
15. Sharma V. K., Chattopadhyay M. K. and Roy S. B., *J. Phys. Condens. Matter* **20**, 425210 (2008).
16. Chattopadhyay M. K., et al., *J. Appl. Phys.* **108**, 073909 (2010).
17. V. K. Sharma et al., *J. Phys.: Condens. Matter* **22**, 486007 (2010).
18. Sharma V. K. et al., *Phys. Rev.* B **82**, 172411 (2010).
19. Manekar M., Roy S. B., and Chaddah P., *J. Phys.: Condens. Matter* **12**, L409 (2000).
20. Sharma V. K. et al., *J. Phys. Condens. Matter* **22**, 016008 (2010).
21. Sharma V. K. et al., *Appl. Phys. Lett.* **89**, 222509 (2006)
22. McMichael R. D., Ritter J. J., and Shull R. D., *J. Appl. Phys.* **73**, 6946 (1993).
23. Sharma V. K., Chattopadhyay M. K. and Roy S. B., *J. Phys. D: Appl. Phys.* **40**, 1869 (2007).
24. V. K. Sharma et al., *J. Phys. D: Appl. Phys.* **42**, 185005 (2009).
25. Chattopadhyay M. K., Sharma V. K. and Roy S. B., *Appl. Phys. Lett.* **92**, 022503 (2008).
26. Sharma V. K., *Ph. D Thesis,* Homi Bhabha National Institute, Mumbai, 2012.
27. Planes A. et al., *J. Phys.: Condens. Matter* **21,** 233201 (2009)
28. Krenke T. et al., *J. Magn. Magn. Mater.* **310,** 2788 (2007)
29. Manosa L. et al., *Appl. Phys. Lett.* **92,** 012515 (2008)
30. Sharma V. K., Chattopadhyay M. K. and Roy S. B., *J. Phys. D: Appl. Phys.* **43**, 225001 (2010).
31. Sharma V. K. et al., *J. Phys. D: Appl. Phys.* **44**, 145002 (2011).
32. Sharma V. K., Chattopadhyay M. K., and Roy S. B., *J. Phys. :Condens. Matter* **23**, 366001 (2011).
33. Chattopadhyay M. K., Roy S. B., and Chaddah P., Phys. Rev. B. **72**, 180401(R) (2005)
34. Sharma V. K., Chattopadhyay M. K. and Roy S. B., *Phys. Rev.* B **76**, 140401(R) (2007).
35. Debenedetti P. G. and Stillinger F. H., *Nature* **410**, 259 (2001).